Int. J. Solids Structures Vol. 30, No. 22, pp. 3085–3099, 1993
Printed in Great Britain

0020–7683/93 $6.00+ .00

THE LINEARIZED BUCKLING ANALYSIS OF A COMPOSITE BEAM WITH MULTIPLE DELAMINATIONS

Y. B. LIM and I. D. PARSONS
Department of Civil Engineering, 2122 Newmark C.E. Lab., MC 250,
205 North Mathews Steet, Urbana, IL 61801, U.S.A.

(*Received* 21 *July* 1992; *in revised form* 10 *May* 1993)

Abstract—A simple model is described for predicting the linearized buckling load of a composite beam with multiple delaminations. The model employs an energy method and arbitrary assumed displacements. Lagrange multipliers are used to enforce the kinematic constraints and boundary conditions, enabling a variety of support conditions to be studied. The accuracy of the approach is verified by comparing results with previously published data and a series of finite element analyses. The effects of delamination depth and length on the buckling load are investigated in detail for beams with one and two delaminations. Euler or thin film buckling is observed in most cases. However, for a beam with two delaminations located so that there are two laminae of equal thickness, antisymmetric S-shaped buckling modes are observed for certain delamination lengths.

1. INTRODUCTION

The rapidly increasing use of composite materials has led to demands for a better understanding of their mechanical behavior and possible failure mechanisms. One of the most common failure modes is delamination. Delaminations can exist for several reasons. For example, flaws in the production process can introduce foreign objects or gaps between the laminae. They can also occur as a result of impact by external objects during the operational life of the structure, since the resin which binds the laminae together is rather weak. The presence of delaminations reduces the overall stiffness, and thereby lowers the load carrying capacity of the structures. This paper describes a numerical model for rapidly computing the critical loads of beams with multiple delaminations. The model allows the effect of changes in geometric parameters, such as the length and depth of the delaminations, to be examined quickly. An energy method is used, in which the total potential energy is discretized using the Rayleigh–Ritz method, and the continuity requirements and the boundary conditions are enforced using Lagrange multipliers.

A number of researchers have studied delamination buckling in the past. Knauss *et al.* (1980) performed experiments to visualize the failure process. They reported that failure caused by an impact could be divided into two phases. In the first phase, the laminate is impacted by a foreign object and the resulting effect is interlaminar separation. In the second phase, the laminate could buckle under the effect of applied loads and experience further delamination growth. The same workers (Chai *et al.*, 1981) proposed a one-dimensional model to describe the growth of delaminations in a beam using the fracture energy of the material. They divided the delaminated beam into four regions using the delamination as the boundary. Kinematic continuity and equilibrium conditions were satisfied between adjoining regions. They presented two models: a simple thin film model in which the delamination divides the beam into a very thin and a very thick region, and a general model where the delamination divides the beam into two regions of approximately equal thickness. Simitses *et al.* (1985) used the same four region model to predict the critical loads for delaminated homogeneous beams. The effect of delamination position, size and thickness on the critical loads were studied in detail for simply-supported and clamped boundary conditions. The characteristic equations required for the solution of the eigenvalue problem were derived from the principle of existence of an adjacent equilibrium position.

Several researchers (Chen, 1991; Kardomateas and Schmueser, 1988) have incorporated the effect of transverse shear into their studies. Chen (1991) derived the equilibrium equations for each lamina from the variational energy principle. Compatibility, kinematic

continuity and equilibrium requirements were then imposed between appropriate regions. Kardomateas and Schmueser (1988) used the perturbation technique to derive the equations for the critical loads and the postbuckling deflections. The instability problem arising from local buckling or mixed mode buckling involving local and global modes was also studied.

Sheinman and Soffer (1991) proposed a geometrical nonlinear model for tracing the equilibrium path into the postbuckling region. A finite difference scheme incorporating Newton's method was used to solve the nonlinear equilibrium equations. The influence of the delamination ratio, initial imperfections and the stretching–bending effect on the postbuckling characteristics of the beam was studied.

The problem of a single delamination in a circular plate has been studied by Bottega and Maewal (1983), Larsson (1991a), Yin (1985), and Yin and Fei (1988). As a result of the axisymmetric nature of the problem, the plate is reduced to a two dimensional plane, and a three region model adopted. These studies focussed on the postbuckling behavior of the plate, and investigated the initiation and stability of the growth of the delamination.

Perhaps because of its relative complexity, the problem of multiple delaminations has not yet been as extensively studied as the solitary case. However, there have been some notable attempts to solve this more general problem. Wang *et al.* (1985a, b) developed models and performed experiments to investigate the buckling stability of, and delamination growth in, random short fiber composites (which are essentially homogeneous, orthotropic materials). Two analytical techniques were employed: a Rayleigh–Ritz method for studying the single delamination case, and the finite element method for solving the plane elasticity problem associated with multiple delaminations. Although the analysis was found to be in good agreement with the experimental results, this study was restricted to symmetric buckling modes. Larsson (1991b) considered multiple delaminations under axisymmetric geometry and loading conditions. The model allowed for non-frictional contact between the layers and anisotropic material behavior. The thin film approximation was used, which in effect neglects bending deformation in the undamaged portions of the plate. Kutlu and Chang (1992) have perhaps presented the most extensive analytical and experimental study to date on multiple delaminations. A finite element model was developed that modeled the collapse of delaminated plates, and included delamination growth and contact between the various layers. It should be noted that this work examined the collapse of the plate, rather than the linearized buckling problem per se. Most recently, Lee *et al.* (1993) employed the finite element method to compute the buckling loads and modes of a plate with multiple delaminations using a layer wise plate theory.

The research reported in this paper has three objectives. First, to develop a simple mathematical model that can be used to perform quick parametric studies of the buckling of composite beams with multiple delaminations. Second, to verify the model by comparisons with solutions generated using the finite element method and results published elsewhere. Third, to use this model to investigate the linearized buckling behavior of a beam with several delaminations. The paper is organized as follows. Section 2 describes the model employed. The use of Lagrange multipliers in conjunction with an energy method for computing the buckling loads of structures is summarized in Section 3. Section 4 discusses the energy formulation for the delaminated beam in detail. Some results are presented in Section 5, and Section 6 contains the conclusions.

2. PROBLEM DEFINITION

The model of the delaminated beam employed in this study shown in Fig. 1 is similar to that used by Chai *et al.* (1981) for the case of single delamination. A beam of length L and thickness t has k delaminations of equal length l_k lying along a plane parallel to the undeformed length of the beam. The delaminations are located symmetrically so that the lengths of the undelaminated sections of the beam are equal (i.e. $l_{k+2} = l_{k+3}$). The depth of each delamination is d_i, $i = 1, 2, \ldots, k$, and the thickness of each lamina is denoted by t_i where $i = 1, 2, \ldots, k+1$. The beam can therefore be divided into $k+3$ regions as shown in Fig. 1. Normalized lamina thickness, $\bar{t}_i$, delamination depth, $\bar{d}_i$, and length, $\bar{l}_i$, are introduced such that

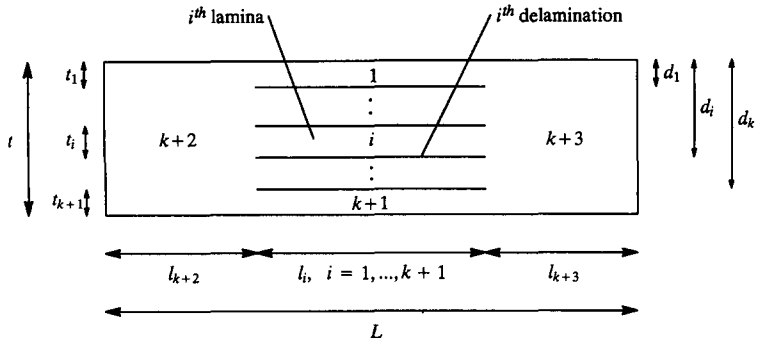

Fig. 1. Model of a beam with k delaminations.

$$\bar{t}_i = \frac{t_i}{t}, \quad i = 1, 2, \ldots, k+1, \tag{1}$$

$$\bar{d}_i = \frac{d_i}{t}, \quad i = 1, 2, \ldots, k \tag{2}$$

and

$$\bar{l}_i = \frac{l_i}{L}, \quad i = 1, 2, \ldots, k. \tag{3}$$

A Cartesian coordinate system (s_i, z_i) is placed at the left end of each of the $k+3$ regions, where the s_i axis corresponds to the neutral axis of the region (see Fig. 2). Moreover, u_i and w_i, $i = 1, 2, \ldots, k+3$, denote the in-plane and transverse displacement of the mid-plane of each region, respectively.

The beam is composed of an arbitrary number of orthotropic laminae. The conventional notation is used to indicate the stacking sequence of the plies; for example, [0/45/90] denotes ply orientations of 0°, 45° and 90°. In addition, the double slash notation introduced by Kutlu and Chang (1992) will be employed to identify the locations of the delaminations in composite beams. Thus, [0//45/90] indicates the presence of a delamination between the 0° and 45° plies. Since each lamina behaves as a linear elastic material, any nonlinearity is purely geometrical. The length and the thickness of each region are such that Euler–Bernoulli beam theory is applicable throughout. An axial compressive load of magnitude P is applied at each end of the beam as shown in Fig. 2. Any geometric boundary condition may be applied at either end of the beam, such as fixed, simply-supported, or free.

3. ENERGY METHODS FOR APPROXIMATING BUCKLING LOADS

Energy methods present approximate but simple tools for solving buckling problems. The fundamental principle is that a static conservative system is in a state of stable equilibrium if, and only if, the value of its potential energy is a relative minimum. To demonstrate the basic idea, let the total potential energy of a conservative mechanical system be V, and

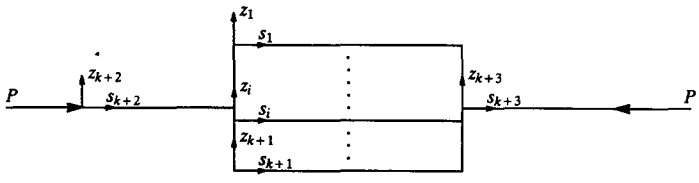

Fig. 2. Coordinate systems and neutral axes of the delaminated beam.

assume that the displacements in the structure can be represented by several coordinate functions $a_1, a_2, \ldots, a_n$, so that

$$V = V(a_1, a_2, \ldots, a_n). \tag{4}$$

Equilibrium is satisfied when V is stationary, i.e. when

$$\frac{\partial V}{\partial a_i} = 0, \quad \text{for all } i = 1, 2, \ldots, n. \tag{5}$$

The Rayleigh–Ritz method approximates the buckling load in those cases in which the exact solution of the underlying differential equation becomes too cumbersome (Bleich, 1952; Brush and Almroth, 1975). In this approach, the buckled shape of the structure is assumed to be a linear combination of several functions. The critical load is then obtained by minimizing the total potential energy with respect to the unknown coefficients a_i, since this will give the loads at which the assumed deformation is in equilibrium with the applied loads. Thus, any prebuckling deformation is implicitly neglected. The successful application of the Rayleigh–Ritz method hinges largely on the appropriate choice of the coordinate functions. In general, each term of the expansion should satisfy the geometric boundary conditions and kinematic constraints associated with the problem, which limits the choice of functions in many cases.

However, if Lagrange multipliers are included in the energy expression, each term of the expansion does not need to satisfy the geometric boundary conditions or constraints (Budiansky and Hu, 1945; Bleich, 1952). This can greatly simplify the selection of the assumed displaced shape. The procedure is implemented by introducing additional terms into the expression for the total potential energy of the system in the form of the unknown Lagrange multipliers multiplied by functions that express the required constraints. These additional terms are equivalent to the change in potential of the restraining forces in their movement through the violated boundary conditions.

The final total potential energy of the system. $\bar{V}$, then becomes

$$\bar{V} = V(a_1, a_2, \ldots, a_n) - \lambda_1 f_1 - \lambda_2 f_2 - \cdots - \lambda_r f_r, \tag{6}$$

where λ_i are the Lagrange multipliers, and the r equations

$$f_i(a_1, a_2, \ldots, a_n) = 0 \tag{7}$$

express the kinematic constraint conditions which are not satisfied by the selected coordinate functions. The total number of unknowns is $(n+r)$, which are then determined by solving the n equations given by

$$\frac{\partial \bar{V}}{\partial a_i} = 0, \quad \text{for all } i = 1, \ldots, n, \tag{8}$$

and the r equations obtained from

$$\frac{\partial \bar{V}}{\partial \lambda_i} = 0, \quad \text{for all } i = 1, \ldots, r. \tag{9}$$

This generally leads to an eigenvalue problem, in which the eigenvalues give the buckling loads, and the corresponding buckling modes are given by the eigenvectors.

4. ENERGY FORMULATION FOR DELAMINATED BEAMS

To apply the energy method to the delaminated beam, both the geometric boundary conditions and kinematic continuity between the beam regions must be enforced using Lagrange multipliers. For example, appropriate boundary conditions at the left end of the beam (i.e. at $s_{k+2} = 0$) would be

$$u_{k+2} = w_{k+2} = 0 \tag{10}$$

for simple supports, and

$$u_{k+2} = w_{k+2} = \frac{\partial w_{k+2}}{\partial s} = 0 \tag{11}$$

for clamped supports. Constraints must be enforced at the junctions of the $k+3$ regions to ensure that plane sections of the beam remain plane. At the junction between regions 1, $2, \ldots, k+1$ and $k+2$, the appropriate kinematic continuity conditions are

$$w_1|_{s_1=0} = \cdots = w_{k+1}|_{s_{k+1}=0} = w_{k+2}|_{s_{k+2}=l_{k+2}}, \tag{12}$$

$$\left.\frac{\partial w_1}{\partial s}\right|_{s_1=0} = \cdots = \left.\frac{\partial w_{k+1}}{\partial s}\right|_{s_{k+1}=0} = \left.\frac{\partial w_{k+2}}{\partial s}\right|_{s_{k+2}=l_{k+2}} \tag{13}$$

and

$$u_i|_{s_i=0} = u_{k+2}|_{s_{k+2}=l_{k+2}} - \frac{t}{2}(1+\bar{t}_i-2\bar{d}_i)\left.\frac{\partial w_{k+2}}{\partial s}\right|_{s_{k+2}=l_{k+2}}, \quad i = 1, \ldots, k+1. \tag{14}$$

Under the usual assumptions made for Euler–Bernoulli beams, the potential energy of the composite beam can be divided into four parts: the axial strain energy

$$U_a = \sum_{i=1}^{k+3} \frac{1}{2} \int_0^{l_i} A_{11}^{(i)} \left(\frac{\partial u_i}{\partial s_i}\right)^2 \mathrm{d}s_i, \tag{15}$$

the bending strain energy

$$U_b = \sum_{i=1}^{k+3} \frac{1}{2} \int_0^{l_i} D_{11}^{(i)} \left(\frac{\partial^2 w_i}{\partial s_i^2}\right)^2 \mathrm{d}s_i, \tag{16}$$

the strain energy due to coupling between bending and stretching

$$U_c = -\sum_{i=1}^{k+3} \int_0^{l_i} B_{11}^{(i)} \frac{\partial u_i}{\partial s_i} \frac{\partial^2 w_i}{\partial s_i^2} \mathrm{d}s_i, \tag{17}$$

and the potential energy of the applied load

$$\Omega = \sum_{i=1}^{k+3} \frac{1}{2} \int_0^{l_i} P_i \left(\frac{\partial w_i}{\partial s_i}\right)^2 \mathrm{d}s_i, \tag{18}$$

where $A_{11}^{(i)}$, $B_{11}^{(i)}$ and $D_{11}^{(i)}$ are the familiar stretching, coupling and bending stiffness, respectively, for region i of the beam. These stiffnesses are defined in terms of the axial stiffnesses of the individual laminae in each laminated beam section [see Whitney (1987), for example, for more details]. Note that, if attention is restricted to an isotropic, homogeneous material,

$$A_{11}^{(i)} = EA_i, \tag{19}$$

$$B_{11}^{(i)} = 0 \tag{20}$$

and

$$D_{11}^{(i)} = EI_i, \tag{21}$$

where E is Young's modulus, and A_i and I_i are the cross-sectional area and moment of inertia of region i, respectively. Hence,

$$V = U_a + U_b + U_c - \Omega. \tag{22}$$

In eqn (18), P_i represents the axial load carried in each region of the beam. Since prebuckling bending deformations are neglected,

$$P_{k+2} = P_{k+3} = P \tag{23}$$

and

$$P_i = \frac{A_{11}^{(i)}}{A_{11}^{(k+2)}} P, \quad i = 1, 2, \ldots, k+1, \tag{24}$$

which reduces to

$$P_i = P\bar{t}_i, \quad i = 1, 2, \ldots, k+1, \tag{25}$$

for an isotropic, homogeneous material. Furthermore, only the bending deformation is considered in eqn (18). This is because buckling is a bending phenomenon and the axial deformation that occurs in the equilibrium state before buckling has no bearing on the evaluation of the critical loads.

Fourier series and quadratic polynomials are used to discretize the energy expression. The assumed displaced shapes in each of the $k+3$ regions of the beam are

$$w_i(s_i) = \sum_{m=1}^{m=6} A_{m_i} \cos\frac{m\pi s_i}{l_i} + \sum_{n=1}^{n=6} B_{n_i} \sin\frac{n\pi s_i}{l_i} + A_{0_i} s_i + B_{0_i} \tag{26}$$

and

$$u_i(s_i) = C_{2_i} s_i^2 + C_{1_i} s_i + C_{0_i}. \tag{27}$$

Evaluating the first derivative of the potential energy with respect to the unknown geometric coordinates and Lagrange multipliers produces the generalized eigenvalue problem

$$[A]\{\phi\} = P_{\text{crit}}[B]\{\phi\}, \tag{28}$$

where P_{crit} is the critical buckling load. The unknown coordinate functions which describe the assumed displaced shape are obtained from the eigenvector $\{\phi\}$. Both of the matrices $[A]$ and $[B]$ are symmetric; however, they may not be positive definite. The generalized eigenvalue problem was solved using an IMSL routine that uses the QZ algorithm of Moler and Stewart (1973).

Table 1. Normalized buckling loads for a simply-supported beam with a single delamination, $\bar{d}_1 = 0.40$

$\bar{l}_1$	Energy method	Abaqus	Simitses *et al.* (1985)
0.20	0.9997	0.9997	0.9997
0.40	0.9902	0.9902	0.9902
0.60	0.9198	0.9197	0.9198
0.80	0.7264	0.7264	0.7264

5. RESULTS

This section presents results obtained using the model described above to study the buckling behavior of beams with one and two delaminations. Comparisons are made with results computed using the Abaqus finite element code, thin film buckling loads (Chai *et al.*, 1981), and data previously published by Simitses *et al.* (1985), Kutlu and Chang (1992), and Lee *et al.* (1993).

5.1. *Single delamination*

To verify the accuracy of the model employed in this study, the finite element code Abaqus was used to compute the buckling loads of selected beams with a single delamination. Attention here is restricted to beams composed of an isotropic, homogeneous material. Table 1 shows the numerical results obtained with $\bar{d}_1 = 0.4$ for simply-supported boundary conditions using the energy method and Abaqus, as well as those published in Simitses *et al.*, (1985). The table shows the normalized buckling load, $\bar{P}_{\text{crit}}$, defined as

$$\bar{P}_{\text{crit}} = \frac{P_{\text{crit}}}{P_{\text{Euler}}}, \tag{29}$$

where P_{Euler} is the Euler buckling load for the undelaminated beam. Clearly there is excellent agreement between the various methods, with any differences being negligible for all practical purposes.

Figures 3 and 4 show plots of the normalized buckling load, $\bar{P}_{\text{crit}}$, versus normalized delamination length, $\bar{l}_1$, for beams clamped and simply supported at both ends, respectively, with single symmetric delaminations at various depths. Also shown are the results predicted using the thin film model (Chai *et al.*, 1981), whereby

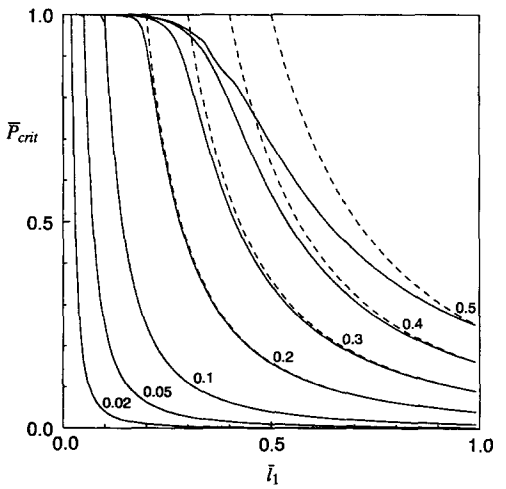

Fig. 3. Normalized buckling loads for a clamped beam with a single symmetric delamination for various values of $\bar{d}_1$ (dashed lines show thin film predictions).

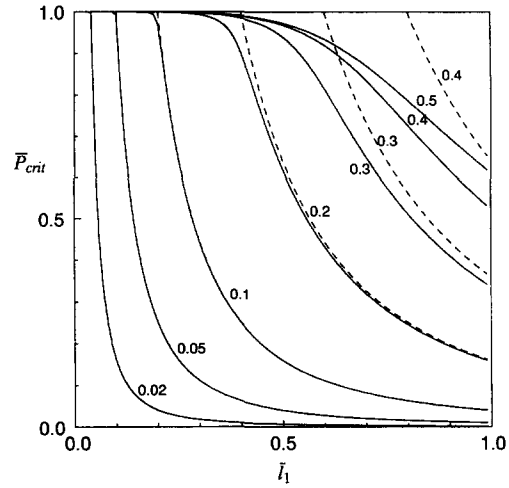

Fig. 4. Normalized buckling loads for a simply-supported beam with a single symmetric delamination for various values of $\bar{d}_1$ (dashed lines show thin film predictions).

$$P_{\text{crit}} = \frac{E\pi^2}{3}\left(\frac{d_1}{l_1}\right)^2 t, \tag{30}$$

for a beam of unit width.

The data shown in Figs 3 and 4 are generally in good agreement with the results presented in Simitses *et al.* (1985). A transition between Euler and thin film buckling is observed as the delamination length is increased. As expected, the thin film model gives accurate results for the shallow delaminations ($\bar{d}_1 \leqslant 0.1$). However, for deeper delaminations, there is a range of lengths for which there is a transition between the thin film and Euler buckling loads. For the simply-supported case, the thin film buckling formula gives poor results when $\bar{d}_1 = 0.4$ and 0.5.

There is one discrepancy between the results shown in Fig. 3 for the clamped boundary conditions and those shown in Simitses *et al.* (1985). For $\bar{d}_1 = 0.5$, the energy method predicts a suspicious kink in the plot of $\bar{P}_{\text{crit}}$ versus $\bar{l}_1$ for $0.35 \leqslant \bar{l}_1 \leqslant 0.4$. Further investigations revealed that this was due to the presence of an antisymmetric S-shaped buckling mode that is often the second mode. Figure 5 shows a plot of the critical loads associated with the first two buckling modes for $\bar{d}_1 = 0.5$. There is an interchange between the lowest

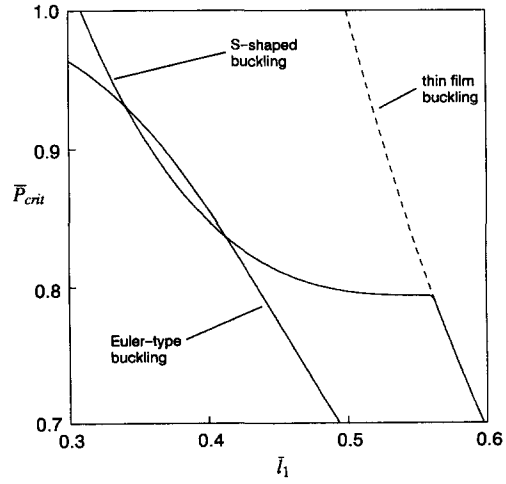

Fig. 5. Critical loads for the first two buckling modes of a clamped beam with a single symmetric delamination; $\bar{d}_1 = 0.5$.

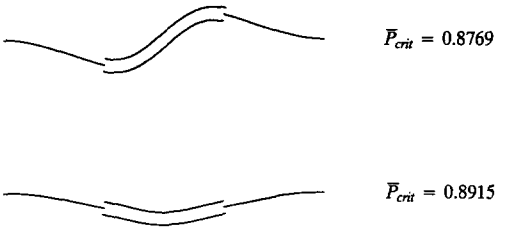

Fig. 6. First two buckling mode shapes for a clamped beam with a single symmetric delamination: $\bar{l}_1 = 0.375$, $\bar{d}_1 = 0.5$.

modes for $0.35 \leqslant \bar{l}_1 \leqslant 0.4$ that causes the kink seen in Fig. 3. Figure 6 shows these two modes for $\bar{l}_1 = 0.375$ (the buckling modes are depicted by plotting the neutral axes of the different laminae), and reveals the S-shaped buckling pattern, which does not involve contact between the laminae. These observations were verified using Abaqus, and were also noted in Lee *et al.* (1993).

One advantage of the energy method developed in this paper is the ease with which different boundary conditions can be considered. Figure 7 shows normalized buckling loads for a beam with clamped, simply-supported boundary conditions. The trends are fairly similar to those observed for the purely simply-supported case. Euler buckling controls for short delaminations, whereas the thin film model works well for long, shallow delaminations. However, for $\bar{d}_1 = 0.4$ and 0.5, there is no agreement with the thin film predictions.

5.2. *Two delaminations*

Perhaps the most useful feature of the model described here is its ability to rapidly study the linearized buckling of beams with multiple delaminations. This section focuses on beams with two delaminations and clamped and simply-supported boundary conditions, while still only considering isotropic, homogeneous materials. One of the problems associated with this situation is the large amount of data that can be generated by varying the depths of the two delaminations. Rather than considering every possible combination, the following results attempt to demonstrate the different types of buckling behavior that have been observed.

To further verify the proposed method, Table 2 shows a comparison between the results generated by Abaqus and the energy method for various delamination lengths with $\bar{d}_1 = 0.3$ and $\bar{d}_2 = 0.6$. Once again, the agreement is excellent. Figure 8 shows plots of the normalized critical load versus normalized delamination length for a beam clamped at each end. The depth $\bar{d}_2$ was held fixed at 0.6, while $\bar{d}_1$ was varied from 0.1 to 0.9 in increments of 0.1 (excluding 0.6). Also shown are the critical loads from the thin film analysis for

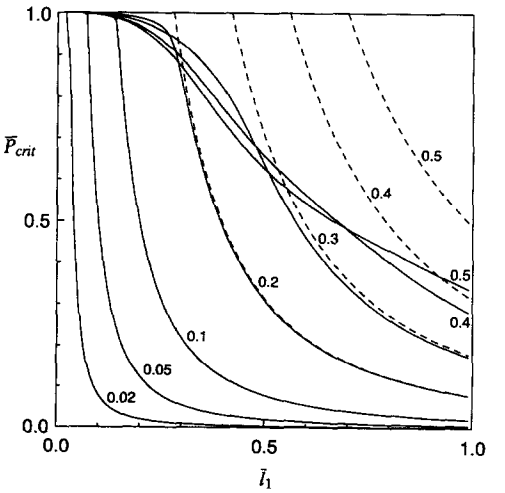

Fig. 7. Normalized buckling loads for a clamped, simply-supported beam with a single symmetric delamination for various values of $\bar{d}_1$ (dashed lines show thin film predictions).

Table 2. Normalized buckling loads for a clamped beam with two delaminations, $\bar{d}_1 = 0.30$, $\bar{d}_2 = 0.60$

$\bar{l}_1 = \bar{l}_2$	Energy method	Abaqus
0.20	0.8939	0.8940
0.40	0.5054	0.5056
0.60	0.2374	0.2375
0.80	0.1374	0.1375

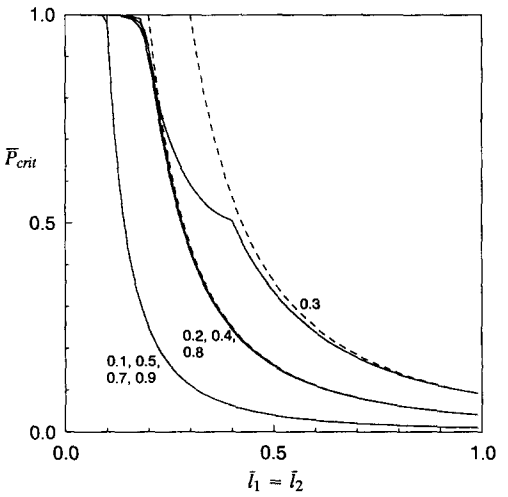

Fig. 8. Normalized buckling loads for a clamped beam with two delaminations for various values of $\bar{d}_1$; $\bar{d}_2 = 0.60$ (dashed lines show thin film predictions for $\bar{d}_1 = 0.1, 0.2, 0.3$).

$\bar{d}_1 = 0.1$, 0.2, and 0.3. The results for the two delaminations in Figure 8 basically fall on three distinct lines. First, when $\bar{d}_1 = 0.1$, 0.5, 0.7 and 0.9, the buckling load is predicted by the thin film results for $\bar{d}_1 = 0.1$ or the Euler buckling results, depending on the delamination length. Similarly, when $\bar{d}_1 = 0.2$, 0.4, and 0.8, the results agree well with thin film buckling for $\bar{d}_1 = 0.2$ or the Euler load. Finally, for $\bar{d}_1 = 0.3$, the buckling load is given either by the Euler load for $\bar{l}_k \leqslant 0.2$ and the thin film load for $\bar{d}_1 = 0.3$ when $\bar{l}_k \geqslant 0.4$. A transition zone appears to exist for $0.2 < \bar{l}_k < 0.4$.

The first two of these observations can be explained in the following manner. Consider Fig. 9, which shows sketches of the beam for $\bar{d}_1 = 0.2$, 0.4, 0.8 and $\bar{d}_2 = 0.6$. In each case, the smallest lamina thickness is 0.2. Therefore, for sufficiently large values of $\bar{l}_k$, the critical load will be controlled by the buckling of the thinnest lamina, i.e. by the thin film buckling load for $\bar{d}_1 = 0.2$. However, when $\bar{d}_1 = 0.4$, the thin film will be the middle lamina, and therefore thin film buckling will involve contact with either of the other laminae. The

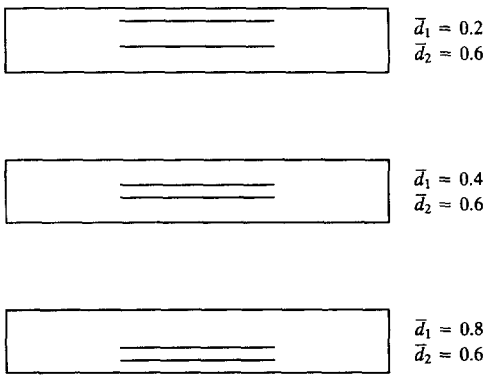

Fig. 9. Geometry of the beam with two delaminations for $\bar{d}_1 = 0.2$, 0.4, 0.8, and $\bar{d}_2 = 0.6$.

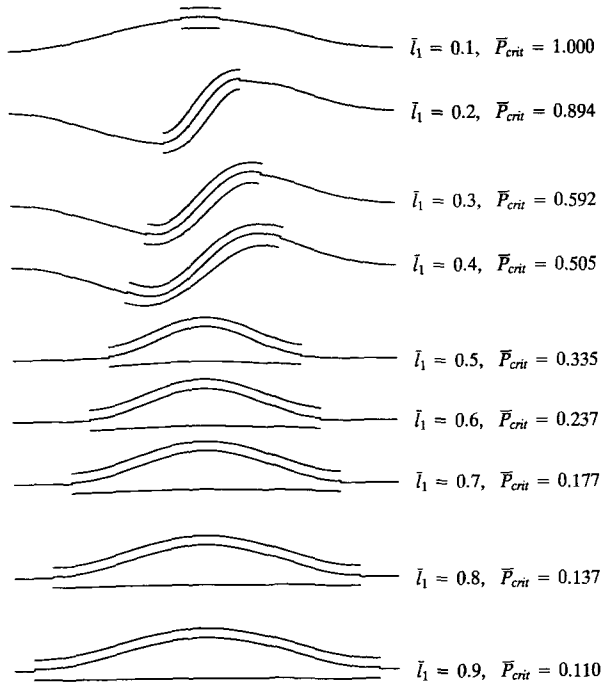

Fig. 10. Buckling mode shapes for the clamped beam with two delaminations: $\bar{d}_1 = 0.3$, $\bar{d}_2 = 0.6$.

linearized buckling analysis presented in this paper cannot model this contact, and further computations would be necessary to fully understand the collapse of this geometry. A similar explanation can be made for $\bar{d}_1 = 0.1$, 0.5, 0.7, and 0.9.

The case $\bar{d}_1 = 0.3$, $\bar{d}_2 = 0.6$ is particularly interesting. Figure 10 shows plots of the buckling modes for various values of $\bar{l}_k$ between 0.1 and 0.9. Three distinct patterns can be seen: the Euler mode for $\bar{l}_k = 0.1$, S-shaped buckling for $0.2 \leqslant \bar{l}_k \leqslant 0.4$, and thin film buckling for $\bar{l}_k \geqslant 0.5$. Thus, the transition between Euler and thin film buckling observed in Fig. 8 is associated with the S-shaped buckling shown in Fig. 10. Furthermore, this buckling pattern generally involves contact between the laminae, and so a more complex model would be required to investigate the postbuckling behavior further. Detailed parameter studies have shown that the S-shaped buckling only occurs for the two delamination case for certain values of $\bar{l}_k$ when the thickness of two of the laminae are equal and lie in a particular range. Figure 11 shows plots of the buckling load versus delamination length for

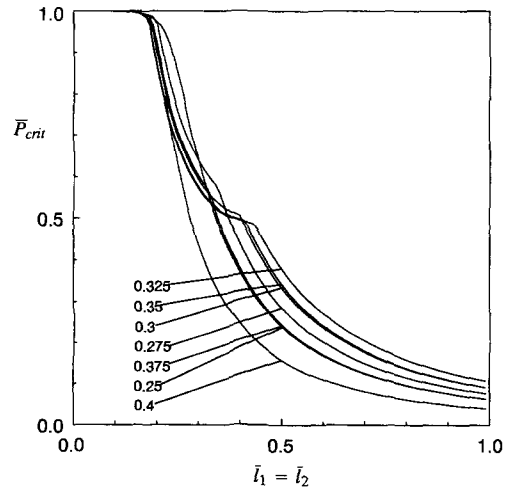

Fig. 11. Normalized buckling loads for a delaminated clamped beam with two lamina of equal thickness for various values of $\bar{d}_1$; $\bar{d}_2 = 2\bar{d}_1$.

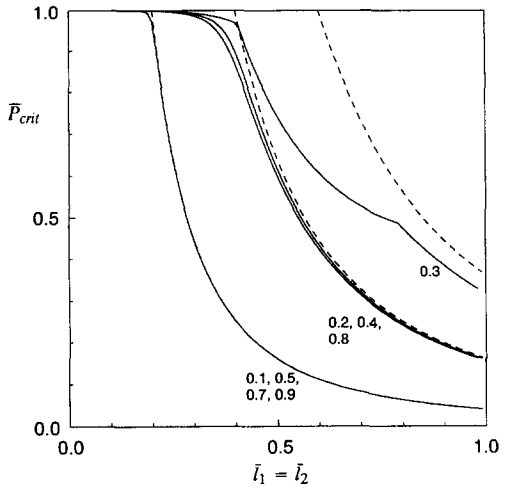

Fig. 12. Normalized buckling loads for a simply-supported beam with two delaminations for various values of $\bar{d}_1$; $\bar{d}_2 = 0.60$ (dashed lines show thin film predictions for $\bar{d}_1 = 0.1, 0.2, 0.3$).

different geometries with laminae of equal thickness. S-shaped buckling is observed to occur for values of $\bar{d}_1 = \bar{d}_2 = 0.275$ to $\bar{d}_1 = \bar{d}_2 = 0.375$ when $\bar{l}_k$ lies roughly between 0.2 and 0.45.

Figures 12, 13 and 14 show the results of a similar study of a beam simply supported at each end. Figure 12 contains plots of buckling load versus delamination length for $\bar{d}_2 = 0.6$ and various values of $\bar{d}_1$. Once again, three types of buckling are observed. The Euler and thin film buckling loads are closely followed when $\bar{d}_1 = 0.1, 0.2, 0.4, 0.5, 0.7, 0.8$ and 0.9 for the same reasons as in the clamped case discussed above. For $\bar{d}_1 = 0.3$, a transition between Euler and thin film buckling is again observed which is associated with S-shaped buckling. Figure 13 shows the mode shapes for different values of $\bar{l}_k$, and highlights the three types of buckling. Figure 14 demonstrates that S-shaped buckling can occur for geometries with two laminae of equal thickness over a range of delamination lengths. For the simply-supported boundary conditions, $\bar{l}_k$ must lie between 0.45 and 0.85 for this to occur.

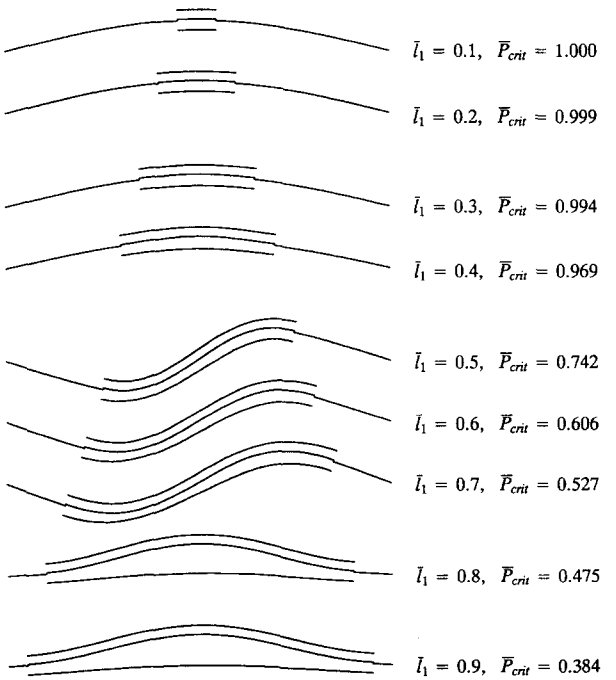

Fig. 13. Buckling mode shapes for the simply-supported beam with two delaminations: $\bar{d}_1 = 0.3$, $\bar{d}_2 = 0.6$.

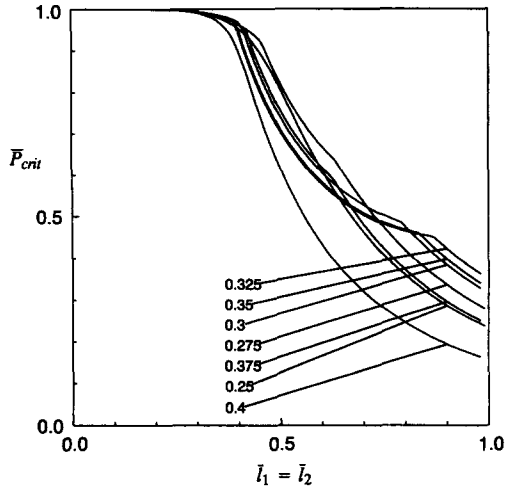

Fig. 14. Normalized buckling loads for a delaminated simply-supported beam with two laminae of equal thickness for various values of $\bar{d}_1$; $\bar{d}_2 = 2\bar{d}_1$.

5.3. *Multiple delaminations in composite beams*

So far, attention has been restricted to beams composed of an isotropic, homogeneous material. The large number of material and geometric parameters associated with delaminated composite beams make a generic study of the buckling behavior of this type of structure extremely difficult. Therefore, in this section, the proposed model is compared to results published by other researchers to highlight the strengths and weaknesses of the method.

Figure 15 shows plots of the normalized buckling loads for three different composite beams computed using the energy method and Abaqus. There is excellent agreement between the two methods for the $[0_4//0_{16}]$ and the $[0_4//(\pm 45)_6/0_4]$ lay-ups; however, as the delamination length increases, differences arise for the $[0/45/0//(45/0)_3/45]$ case. Further investigation revealed that this was caused by prebuckling deformations resulting from the nonzero coupling stiffnesses of the undelaminated beam sections, which are explicitly neglected by the classical linearized buckling analysis employed in this paper. Apparently, there is a range of geometries and ply lay-ups for which this coupling effect will lead to errors in the predicted buckling loads for all methods based on classical linearized analysis.

Some of the geometries considered in Fig. 15 can be used to compare the results of the proposed model with those presented in Kutlu and Chang (1992). For example, Kutlu and Chang state that the $[0_4//0_{16}]$ beam with $\bar{l}_1 = 0.375$ "buckled at a load near 3,500 lbf/in."

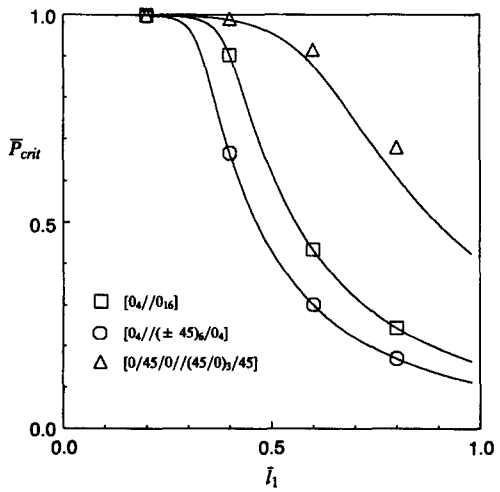

Fig. 15. Normalized buckling loads for three composite delaminated simply-supported beams (the solid lines and symbols denote results produced by the energy method and Abaqus, respectively).

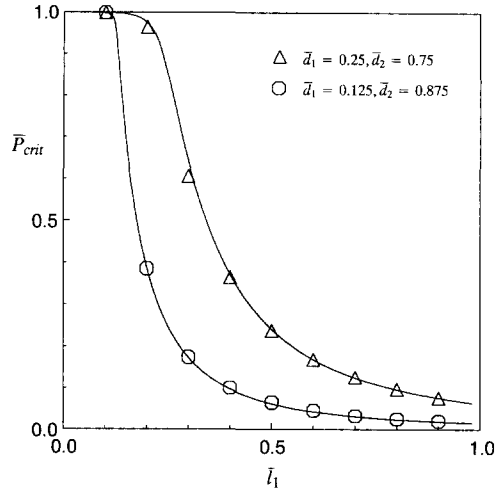

Fig. 16. Normalized buckling loads for two composite delaminated simply-supported beams [the solid lines and symbols denote results produced by the energy method and Lee *et al.* (1993), respectively].

The linearized buckling load computed using the energy method was 3,980 lbf in^{-1} (compared to 3,960 lbf in^{-1} computed using Abaqus). Thus, reasonable agreement is observed between these different methods when it is noted that Kutlu and Chang were performing collapse analyses, rather than calculating the linearized buckling loads directly.

Buckling loads for composite beams with multiple delaminations are reported in Lee *et al.* (1993). Figure 16 shows a comparison between the reported buckling loads and those generated using the energy method for two beams with two delaminations symmetrically located through the thickness. The beams were composed of an orthotropic, homogeneous material, and so are identical to problems solved by Wang *et al.* (1985a, b). Clearly, the two different methods produce almost identical results, and are also in agreement with Wang *et al.* (1985a, b).

6. CONCLUSIONS

An energy method has been developed for computing the linearized buckling loads of delaminated composite beams. The Rayleigh–Ritz method is used in which the displacements in each lamina of the beam are approximated using Fourier series and polynomials. Lagrange multipliers are used to enforce constraints arising from the boundary conditions and the kinematic continuity requirements between the different sections of the beam. The method enables the buckling loads and modes to be rapidly computed for a variety of boundary conditions and a number of delaminations.

The accuracy of the energy formulation was examined by computing the buckling loads for isotropic, homogeneous beams with a single delamination and clamped and simply-supported boundary conditions. The results were observed to compare well with previously published data. In addition, selected results agreed with those generated using the Abaqus finite element package. For the single delamination case, Euler buckling dominates if the delamination is sufficiently short. For longer, shallow delaminations, thin film buckling controls. There is a transition between Euler and thin film buckling for deeper delaminations; when simply-supported boundary conditions were considered, the thin film results gave poor buckling load predictions for deep delaminations (i.e. $\bar{d}_1 \geqslant 0.4$).

Studies of isotropic, homogeneous beams with two delaminations revealed some interesting phenomena. Generally, the linearized buckling load is controlled either by the Euler buckling load if the delaminations are short enough, or by the thin film buckling of the thinnest lamina. It should be noted that this can result in contact between the laminae if the thinnest lamina is not adjacent to the top or bottom surfaces of the beam. If there are two laminae of equal thickness, then there is a range of delamination lengths for which S-shaped buckling occurs, which also involves contact between the layers.

Some comparisons were made between the buckling loads predicted by the energy method for composite beams and those published elsewhere. Generally, good agreement was observed. However, it was also noted that prebuckling bending deformations resulting from the bending–stretching coupling present in unsymmetric lay-ups can sometimes lead to inaccuracies when a classical linearized buckling analysis is used.

Since the results presented in this paper are based on a linearized buckling analysis, no information has been produced related to the postbuckling behavior of the delaminated beams. For the single delamination case, it is well known that thin film buckling is not generally accompanied by the collapse of the entire beam (Yin *et al.*, 1986). Further studies are required to investigate the collapse of the beam with two delaminations, especially in those cases that involve contact between the laminae in the buckling modes.

REFERENCES

Bleich, F. (1952). *Buckling Strength of Metal Structures*. McGraw-Hill, Maidenhead.

Bottega, W. J. and Maewal, A. (1983). Delamination buckling and growth in laminates. *J. Appl. Mech.* **50,** 184–189.

Brush, D. O. and Almroth, B. O. (1975). *Buckling of Bars, Plates, and Shells*. McGraw-Hill, Maidenhead.

Budiansky, B. and Hu, P. C. (1945). The Lagrange multiplier method of finding upper and lower limits to critical stresses of clamped plates. NACA Technical Report No. 1103.

Chai, H., Babcock, C. D. and Knauss, W. G. (1981). One dimensional modeling of failure in laminated plates by delamination buckling. *Int. J. Solids Structures* **17,** 1069–1083.

Chen, H. P. (1991). Shear-deformation theory for compressive delamination buckling and growth. *AIAA Jl* **29,** 813–819.

Kardomateas, G. A. and Schmueser, D. W. (1988). Buckling and postbuckling of delaminated composites under compressive loads including transverse shear effects. *AIAA Jl.* **26,** 337–343.

Knauss, W. G., Babcock, C. D. and Chai, H. (1980). Visualization of impact damage of composite plates by means of the Moiré technique. NASA CR-159261.

Kutlu, Z. and Chang, F.-K. (1992). Modeling compression failure of laminated composites containing multiple through-the-width delaminations. *J. Compos. Mater.* **26,** 350–387.

Larsson, P.-L. (1991a). On delamination buckling and growth in circular and annular orthotropic plates. *Int. J. Solids Structures* **27,** 15–28.

Larsson, P.-L. (1991b). On multiple delamination buckling and growth in composite plates. *Int. J. Solids Structures* **27,** 1623–1637.

Lee, J., Guerdal, Z. and Hayden Griffen, O. (1993). Layer-wise approach for the bifurcation problem in laminated composites with delaminations. *AIAA Jl* **31,** 331–338.

Moler, C. and Stewart, G. W. (1973). An algorithm for generalized matrix eigenvalue problems. *SIAM J. Numer. Anal.* **10,** 241–256.

Sheinman, I. and Soffer, M. (1991). Post-buckling analysis of composite delaminated beams. *Int. J. Solids Structures* **27,** 639–646.

Simitses, G. J., Sallam, S. and Yin, W. L. (1985). Effect of delamination of axially loaded homogeneous laminated plates. *AIAA Jl* **23,** 1437–1444.

Wang, S. S., Zahlan, N. M. and Suemasu, H. (1985a). Compressive stability of delaminated random short-fiber composites. Part i—modeling and methods of analysis. *J. Compos. Mater.* **19,** 296–316.

Wang, S. S., Zahlan, N. M. and Suemasu, H. (1985b). Compressive stability of delaminated random short-fiber composites. Part ii—experimental and analytical results. *J. Compos. Mater.* **19,** 317–333.

Whitney, J. M. (1987). *Structural Analysis of Laminated Anisotropic Plates*. Technomic Publishing.

Yin, W. L. (1985). Axisymmetric buckling and growth of a circular delamination in a compressed laminate. *Int. J. Solids Structures* **21,** 503–514.

Yin, W. L. and Fei, Z. (1988). Delamination buckling and growth in a clamped circular plate. *AIAA Jl* **26,** 438–445.

Yin, W. L., Sallam, S. N. and Simitses, G. J. (1986). Ultimate axial load capacity of a delaminated beam-plate. *AIAA Jl* **24,** 123–128.